https://dx.doi.org/10.1016/j.cej.2022.136947

Design mitochondria-specific fluorescent turn-on probes targeting G-quadruplexes for live cell imaging and mitophagy monitoring study

Meng-Ting She,[a] Jia-Wei Yang,[a] Bo-Xin Zheng,[a,b] Wei Long,[a] Xuan-He Huang,[a] Jun-Ren Luo,[a] Ze-Xin Chen,[a] Ao-Lu Liu,[a] Dong-Peng Cai,[a] Wing-Leung Wong[*,b,c] and Yu-Jing Lu,[*,a,d]

[a] School of Biomedical and Pharmaceutical Sciences, Guangdong University of Technology, Guangzhou 510006, P. R. China.

[b] State Key Laboratory of Chemical Biology and Drug Discovery, Department of Applied Biology and Chemical Technology, The Hong Kong Polytechnic University, Hung Hom, Kowloon, Hong Kong SAR, China.

[c] The Hong Kong Polytechnic University Shenzhen Research Institute, Shenzhen 518057, P. R. China.

[d] Smart Medical Innovation Center, Guangdong University of Technology, Guangzhou 510006, P. R. China.

* Corresponding author

E-mail: luyj@gdut.edu.cn;

E-mail: wing.leung.wong@polyu.edu.hk

Graphical abstract

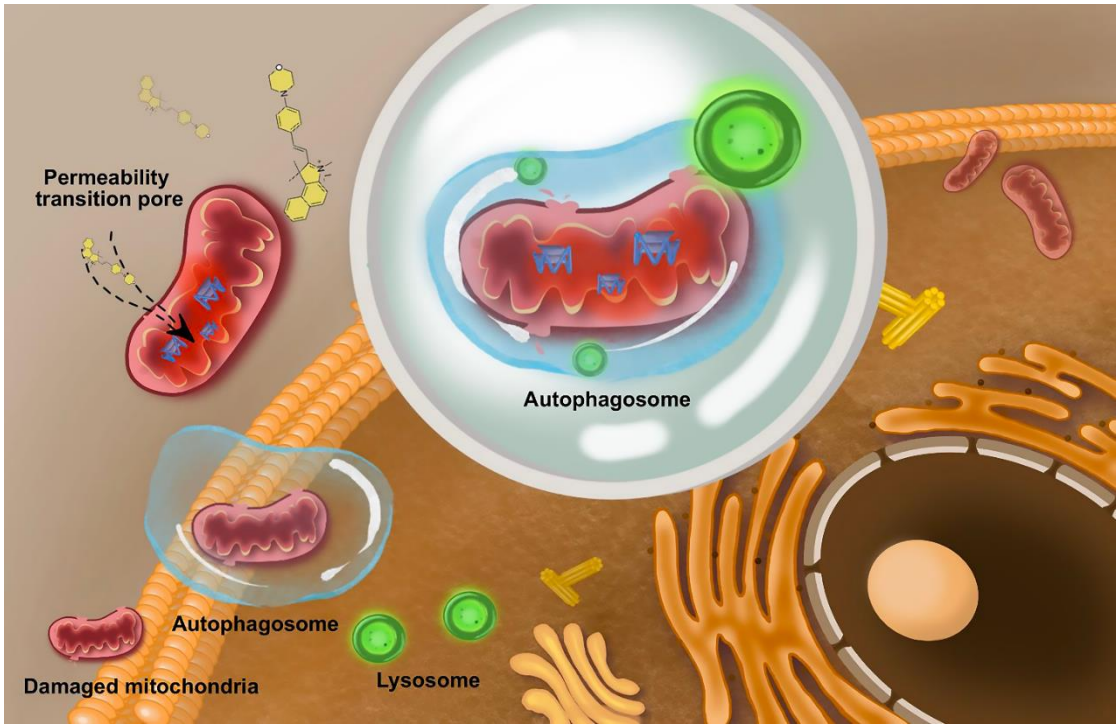

Abstract:

A series of new mitochondrial-selective fluorescent probe was designed and synthesized based on the integration of two planar molecular scaffolds of benzo-indole/indole with a *p*-substituted styrene moiety. The small-sized probes are flexible and rotatable via an ethylene bridge. The restriction of free rotation upon interaction with targeting biomolecules of G-quadruplexes in mitochondria generates strong emission in visible range (575-615 nm). Cell imaging study showed that the ligands are targeting mitochondria but not nucleus. Competition experiments showed that the ligand **BYM** is highly selective towards mitochondrial G4-DNA structures against other non-G4 nucleic acid structures including single-/double-stranded DNA and hairpin. The equilibrium binding constant (K_{eq}) of **BYM** interacting with mitochondrial G4-DNA (mt6363, K_{eq} = 10.8×10^6 M^{-1}) is almost 1000-fold higher than that of mitochondrial double-stranded DNA (K_{eq} = 0.01×10^6 M^{-1}). The probe also showed high sensitivity (LOD = 1.52 nM) and good linear relationship (R^2 = 0.9983) with the mitochondrial G4-DNA. The delivery of **BYM** to mitochondria is not mitochondrial membrane potential dependent but mainly through the permeability transition pore on the mitochondrial inner membrane. In addition, **BYM** exhibits low cytotoxicity against a number of human cancer and noncancerous cells, indicating that **BYM** could be a good ligand for bioorthogonal study in live cells by targeting the mitochondrial G4-DNA structures. In the present study, **BYM** was demonstrated in monitoring the dynamic process of mitochondrial autophagy. The small-sized fluorescent probe possessing high photostability, selectivity and sensitivity targeting mitochondrial G-quadruplexes may able to provide a useful chemical tool for real-time study of mitochondrial functions in live cells.

1. Introduction

Mitochondria are called "energy factories" in eukaryotic cells, which not only regulate cell respiration but also are closely related to the metabolic processes of cells and apoptosis.[1] Mitochondria exhibit dynamic features including fission, fusion and transport during the biological process in cells.[2, 3] Visualizing and tracking mitochondrial dynamics in living cells is crucial because the information about mitochondrial metabolism in areas including illness, physiology, and pharmacology can be observed and monitored real-time. The study of mitochondrial-related process, particularly the mitochondrial autophagy, has been a hot and emerging field in recent years.[4, 5] Mitochondrial autophagy (mitophagy) is a selective autophagy that maintains mitochondrial stability by removing damaged mitochondria and is associated with the development of a variety of diseases such as diabetes,[6] Alzheimer's disease,[7] and multiple tumor diseases.[8-10]

Functionalized fluorescent probes are able to provide convenient means for staining, visualization, and/or quantification of target substrates in a specific organelle of live cells.[11] The development of mitochondria-specific probes is a very important topic.[12-18] In general, there are two classes of fluorescent probes currently available from commercial for imaging and tracking mitochondrial dynamics, which are the classical electrostatic attraction-based cationic mitochondrial probes and reaction-based MitoTracker probes.[19] Traditional electrostatic attraction-based cationic probes, such as Rhodamine 123 (Rho123), accumulate on the inner membrane of healthy mitochondria by electrostatic attraction because healthy mitochondria have a negative potential (-180 to -200 mV).[20] When the mitochondrial membrane potential (MMP) is decreased or destroyed, the probe may detach from the mitochondria and thus limiting their utility in some biological processes such as mitochondrial autophagy.[21] For the reaction-based probes, such as the commercial probe MitoTracker Green, can react with the nucleophilic reagents including the thiol residues of peptides and proteins in mitochondria to form a long-lasting affinity between the probe and the mitochondria.[22] However, these reaction-based probes usually deplete the thiol groups of the biomolecules in the mitochondria and interfere the normal biological function of the cell, which may cause cell death.[23, 24] Therefore, the development of mitochondrial-specific probes with high biocompatibility without interfering with native biochemical processes and enhanced photophysical properties for bioimaging and monitoring of mitochondrial dynamics is a challenging task.

G-quadruplex is a special secondary structure of nucleic acid formed by Hoogsteen hydrogen bond association.[25] It has been reported that these sequences are mainly distributed in the promoter region of proto-oncogenes, chromosomal telomere ends and the untranslated regions of mRNA.[26, 27] The folding and unfolding process of G4s may implicate in the regulation of important biological activity such as cell growth, proliferation, aging and apoptosis, and the occurrence and development of cancers.[28, 29] The mitochondria contain genetic materials that can be transcribed independently of the nucleus and encode 13 proteins important to the respiratory chain, 2 rRNAs and 22 tRNA genes.[30] As mitochondrial genomes do not contain introns and protective proteins, they are more feasibly to form G4-structures.[31] Some studies show that about 200 sequences in the mitochondrial genome could be able to form G4-structures.[32, 33] At present, despite progress has been made in the study of G4-DNA structures in cells and a number of fluorescent probes selective to G4-DNA in cells have been developed,[34] small-molecule based fluorescent probes targeting mitochondrial G4-DNA are rare. To the best of our knowledge, only several mitochondrial G4-DNA probes such as **BMVC-12C-P**, **NCT**, and **IZIN-1** were published.[31, 35, 36] Due to the existence of excessive secondary structures of other nucleic acids in cells, as well as the complicated intracellular environment, the recognition and sensing of intracellular mitochondrial G4-DNA structures with high selectivity and sensitivity is therefore very significant and desirable for the study of the biological function of mitochondrial G4-DNA.[31] The development of small-sized and target-specific fluorescent probes may be able to provide powerful chemical tools for intracellular investigations of mitochondrial G4-DNA.[37-39]

Mitophagy refers to the biological process of selective sequestration of mitochondria by autophagosomes and followed they are delivered to lysosomes for destruction.[4, 5] Mitochondrial DNA (including G4-DNA) damage may induce mitophagy.[40, 41] In this scenario, mitochondrial G4-DNA (mtG4-DNA) could be a potential target for the study of mitophagy.[42] Advancing the cationic small-molecules with special molecular scaffold and functional groups may construct specific fluorescent probes targeting mtG4-DNA against other cellular substrates for visualizing and monitoring the mitophagy process in live cells.[42] G4-structures are generally believed closely associated to diseases such as cancer [43]; however, the mtG4-DNA selective fluorescent probe developed for mitophagy study is still very limited.[44] We have developed a number of fluorescent ligand systems targeting the nuclear G4-DNA substrates.[45-47] In the present study, we designed a series of new and mitochondria-specific fluorescent probes with fluorescent turn-on

mechanism upon binding to mitochondrial G4-DNA in the mitochondria of live cells. The new target-specific sensing probe is able to provide strong fluorescent sensing signal at the red emission range (> 600 nm) with low detection limit at nano-molar level, high photostability, and low cytotoxicity against human cancer and noncancerous cells. The molecular interaction characteristic and selectivity of the probes targeting mtG4-DNA, their biological compatibility and the visualization of mitophagy process in live HeLa cells were investigated.

2. Experimental Section

2.1 Material

All chemicals and reagents were purchased from commercial in AR grade and used without further purification. Tris-HCl buffer was purchased from Aladdin (Shanghai, China). The medium used for cell culture and fetal bovine serum (FBS) were purchased from (Biological Industries). The oligonucleotide sequences used in the present study were purchased from Sangon Biotech (Shanghai, China) and were shown in **Table S1**. Hoechst 33342 was purchased from Beijing Solarbio Science & Technology Co., Ltd. Rho123, LTG, Mito-Tracker Red CMXRos and Annexin V-PE Apoptosis Detection Kit were purchased from Beyotime Biotechnology (Shanghai, China). MitoLite^{TM}-Blue was purchased from ATT Bioquest (USA). Anti-LC3B antibody [ab192890] was purchased from Abcam (USA). Goat Anti-Rabbit IgG (H+L) FITC-conjugated [Cat# S0008] was purchased from Affinity Biosciences (Jiangsu, China). The nucleic acids used were diluted with Tris-HCl buffer (10 mM, pH=7.4) containing 60 mM or 20 mM KCl and followed were denatured at 95 ℃ for 10 min and then slowly cooled down to room temperature to form secondary structures, which were characterized with circular dichroism (CD) according to literature.[31, 48]

2.2 Synthesis and characterization

2.2.1 Preparation of intermediate I

The intermediate **I** (**Scheme S1**) was synthesized by following the reported procedures.[47] 1,1,2-trimethyl-1*H*-benzo[e]indole (1.5 mmol) was dissolved in sulfolane (6 mL) and then iodomethane (4.5 mmol) was added to the reaction mixture. The mixture was then well-stirred and refluxed overnight. After reaction, the mixture was cooled to room temperature. Ethyl acetate (15 mL) was then added to the solution to precipitate the crude products. The crude products were used for further reactions without purification.

2.2.2 Preparation of intermediate II

The synthesis of intermediate **II** (**Scheme S1**) was performed with the same procedures for the preparation of intermediate **I**. In the reaction, 2,3,3-trimethylindolenine was used as the starting material for the synthesis. The crude products of intermediate **II** isolated were used for further reactions without purification.

2.2.3 Preparation of new probes BYM, YM, BYP and YP

The obtained intermediate (**I** or **II**, 1.5 mmol) and the selected benzaldehyde (3 mmol) including 4-morpholinobenzaldehyde and 4-(4-methylpiperazin-1-yl)benzaldehyde were dissolved in ethanol (6 mL) and stirred at 60 ℃ for 8 h. After reaction, the crude product was isolated by removing the solvents and was purified by flash column chromatography to obtain target compounds. The compounds were then confirmed by ^{1}H & ^{13}C NMR and HRMS (**Figure S1-S4**).

2.2.4 (*E*)-1,1,3-trimethyl-2-(4-morpholinostyryl)-1*H*-benzo[e]indol-3-ium (BYM).

Compound **BYM** was isolated as an air stable reddish black solid with 50.4% yield. ^{1}H NMR (400 MHz, DMSO *d*6) δ 8.40 (t, *J* = 12.6 Hz, 2H), 8.25 (d, *J* = 8.9 Hz, 1H), 8.18 (d, *J* = 8.2 Hz, 1H), 8.13 (d, *J* = 9.0 Hz, 2H), 8.02 (d, *J* = 8.9 Hz, 1H), 7.78 (t, *J* = 7.3 Hz, 1H), 7.67 (t, *J* = 7.5 Hz, 1H), 7.41 (d, *J* = 16.0 Hz, 1H), 7.13 (d, *J* = 9.0 Hz, 2H), 4.15 (s, 3H), 3.80 – 3.72 (m, 4H), 3.54 – 3.46 (m, 4H), 2.00 (s, 6H). ^{13}C NMR (101 MHz, DMSO *d*6) δ 181.74 (s), 154.85 (s), 153.09 (s), 140.06 (s), 137.21 (s), 133.91 (s), 133.18 (s), 131.12 (s), 130.48 (s), 128.72 (s), 127.29 (s), 127.00 (s), 124.53 (s), 123.35 (s), 113.97 (s), 113.38 (s), 107.20 (s), 66.28 (s), 53.40 (s), 46.89 (s), 34.52 (s), 26.23 (s). HRMS m/z: calcd for $C_{27}H_{29}N_2O^+$, $[M\text{-}I]^+$ = 397.22744, found 397.22729.

2.2.5 (*E*)-1,3,3-trimethyl-2-(4-morpholinostyryl)-3*H*-indol-1-ium (YM)

Compound **YM** was isolated as an air stable reddish black solid with 53.6% yield. ^{1}H NMR (400 MHz, DMSO *d*6) δ 8.33 (d, *J* = 15.9 Hz, 1H), 8.11 (d, *J* = 9.0 Hz, 2H), 7.79 (dd, *J* = 18.0, 7.4 Hz, 2H), 7.56 (ddd, *J* = 21.8, 10.9, 6.9 Hz, 2H), 7.37 (d, *J* = 15.9 Hz, 1H), 7.12 (d, *J* = 9.1 Hz, 2H), 4.02 (s, 3H), 3.82 – 3.69 (m, 4H), 3.59 – 3.46 (m, 4H), 1.76 (s, 6H). ^{13}C NMR (101 MHz, DMSO *d*6) δ 180.82 (s), 154.96 (s), 154.18 (s), 143.32 (s), 142.48 (s), 134.11 (s), 129.23 (s), 128.52 (s), 124.45 (s), 123.16 (s), 114.50 (s), 113.91 (s), 107.45 (s), 66.27 (s), 51.69 (s), 46.86 (s), 33.96 (s), 26.50 (s). HRMS m/z: calcd for $C_{23}H_{27}N_2O^+$, $[M\text{-}I]^+$ = 347.21179, found 347.21269

2.2.6 (*E*)-1,1,3-trimethyl-2-(4-(4-methylpiperazin-1-yl)styryl)-1*H*-benzo[e]indol-3-ium (BYP)

Compound **BYP** was isolated as an air stable reddish brown solid with 55.1% yield. ^{1}H NMR (400 MHz, DMSO *d*6) δ 8.21 – 8.11 (m, 2H), 8.01 (d, *J* = 9.0 Hz, 1H), 7.95 (d, *J* = 8.2 Hz, 1H),

7.89 (d, *J* = 9.0 Hz, 2H), 7.78 (d, *J* = 8.9 Hz, 1H), 7.54 (t, *J* = 7.2 Hz, 1H), 7.48 – 7.41 (m, 1H), 7.17 (d, *J* = 16.0 Hz, 1H), 6.91 (d, *J* = 9.0 Hz, 2H), 3.92 (s, 3H), 3.35 (s, 4H), 2.44 (s, 4H), 2.16 (s, 3H), 1.76 (s, 6H). ^{13}C NMR (101 MHz, DMSO *d*6) δ 181.92 (s), 153.89 (s), 152.93 (s), 140.04 (s), 137.37 (s), 133.81 (s), 133.24 (s), 131.14 (s), 130.48 (s), 128.74 (s), 127.17 (d, *J* = 18.7 Hz), 124.91 (s), 123.38 (s), 114.56 (s), 113.44 (s), 107.73 (s), 53.50 (s), 45.08 (s), 34.69 (s), 26.18 (s). HRMS m/z: calcd for $C_{28}H_{32}N_3^+$, $[M-I]^+$ = 410.25907, found 410.25878.

2.2.7 (*E*)-1,3,3-trimethyl-2-(4-(4-methylpiperazin-1-yl)styryl)-3*H*-indol-1-ium (YP)

Compound **YP** was isolated as an air stable reddish brown solid with 49.6% yield. ^{1}H NMR (400 MHz, DMSO *d*6) δ 8.31 (d, *J* = 15.8 Hz, 1H), 8.09 (d, *J* = 9.0 Hz, 2H), 7.77 (dd, *J* = 20.0, 7.3 Hz, 2H), 7.55 (tdd, *J* = 14.8, 10.8, 4.2 Hz, 2H), 7.36 – 7.31 (m, 1H), 7.11 (d, *J* = 9.1 Hz, 2H), 4.01 (s, 3H), 3.57 – 3.51 (m, 4H), 2.48 – 2.43 (m, 4H), 2.23 (d, *J* = 7.1 Hz, 3H), 1.76 (s, 6H). ^{13}C NMR (101 MHz, DMSO *d*6) δ 180.63 (s), 154.81 (s), 154.20 (s), 143.25 (s), 134.30 (s), 129.21 (s), 128.38 (s), 124.02 (s), 123.14 (s), 114.38 (s), 114.01 (s), 107.01 (s), 54.72 (s), 51.60 (s), 46.60 (s), 46.07 (s), 33.87 (s), 26.55 (s). HRMS m/z: calcd for $C_{24}H_{30}N_3^+$, $[M-I]^+$ =360.24342, found 360.24407.

2.3 Fluorescence titration and competition study

For the titration assays and competition assays, the compounds were diluted to 0.5 μM using Tris-HCl buffer (10 mM, pH=7.4) with 60 mM KCl. The corresponding spectra data were recorded with a LS-55 fluorescence spectrometer (Perkin Elmer). The limit of detection (LOD) of the compounds was obtained by the fluorescence titration data and estimated based on the formula: LOD = K(S_b/m). In the equation, S_b is the standard deviation of the blank multiple measurements (n = 20), and m is the slope of the calibration curve, which represents the sensitivity of this method. In addition, according to the International Union of Pure and Applied Chemistry (IUPAC), K value is generally taken to be 3. Fluorescence lifetime was tested using a fluorescent spectrophotometer (HORIBA Instruments Incorporated). Fluorescence decay of compounds at emission wavelengths (**BYM**, λ_{em}=615 nm) was monitored in this experiment and a 550 nm filter was used to filter out the clutter.

2.4 UV-vis absorption measurement and titration study

In UV-vis absorption measurement experiments, the solution of the compound dissolved in DMSO were diluted to 15 μM using Tris-HCl buffer (10 mM, pH=7.4) with 60 mM KCl and nucleic acids (0−2.2 μM) were added into the solution. The corresponding spectra data were recorded with a Lambda 25 Spectrophotometer (Perkin Elmer).

2.5 Native polyacrylamide gel electrophoresis (PAGE) assay

Gel electrophoresis studies were carried out with 20% polyacrylamide-bisacrylamide (29:1) gel. The experimental parameters were performed in 1 × TBE buffer under 0 ℃ conditions, 45V for 15 minutes, and 100V for 60 minutes. After the electrophoretic migration, gels were stained with **BYM** (5 μM, 10 min) and **SYBR Gold** (5 μM, 10 min) respectively. Gel imaging was performed on an AlphaImager HP automatic gel imager.

2.6 Circular dichroism (CD)

CD studies were performed on a Chirascan spectrophotometer (Applied Photophysics). The spectra data were collected from 220 nm to 340 nm with a 1 nm bandwidth, a 1 nm step. CD melting measurement was set as a fixed wavelength, while gradually increasing the temperature from 20 to 95 ℃ at 1 ℃/min heating rate.

2.7 Cell culture, cell staining and fluorescence imaging

Human cervical cancer cells (HeLa) were used for fixed cell staining experiments or live cells staining experiments. HeLa cells were cultured in DMEM supplemented with 10% fetal bovine serum and grown in an incubator at 37 °C with 5% CO_2.

For the live cell staining experiments, HeLa cells were cultured in confocal dishes for 24 h and then treated with 5 μM **BYM** for 30 min and 1 μg/mL Hoechst 33342 for 20 min. In the co-localization experiment, HeLa cells in confocal dishes were treated with MitoLite^{TM}-Blue for 1 h and then 5 μM **BYM** for 30 min.

For the competition experiments, the cells in confocal dishes were treated with 5 μM **BYM** for 30 min and 8 μM BRACO-19 for 30 min. In the dimethyl sulfite (DMS) experiment, the live cells were treated with 20 mM DMS for 20 min and then stained with 5 μM **BYM** for 30 min.

For the photobleaching experiments, HeLa cells in the confocal dish were treated with 5 μM **BYM** for 30 min and then images were taken every 3 seconds (λ_{ex} = 561 nm, λ_{em} = 600-700 nm) under the continuous irradiation of excitation wavelength.

For the DNase and RNase digestion experiments, HeLa cells were fixed with pre-cooled methanol for 5 min and treated with 200 unit/mL DNase (or 200 unit/mL RNase) at 37 ℃ for 1 h. After that, the cells were treated with 5 μM **BYM** for 30 min and 1 μg/mL Hoechst 33342 for 20 min.

For the mitochondrial membrane potential (MMP) depolarization experiments, 10 μM CCCP for 20 min or 4% paraformaldehyde for 30 min at 4 ℃ before imaging was used to changed or

vanished the mitochondrial membrane potential.

For the immunofluorescent colocalization assay of **BYM** with LC3 protein, HeLa cells in the confocal dish were fixed in 4% paraformaldehyde/PBST for 15 min, then infiltrated with 0.1% triton X-100/PBST at 37 ℃ for 30 min, and then blocked with 1% BSA/PBST at 37 ℃ for 3 h. Anti-LC3B antibody [ab192890, Abcam] was diluted 1:400 with blocking buffer and incubated for 3 h at 37 °C. Goat Anti-Rabbit IgG (H+L) FITC-conjugated [S0008, Affinity] was diluted 1:300 with blocking buffer and incubated for 3 h at 37 °C. Finally, 5 μM **BYM** was added to the culture dish and incubated for 30 min at 37 ℃.

For real-time mitophagy tracking and co-localization study of **BYM** with LTG, 5 μM **BYM** was added to the culture dish and incubated for 30 min at 37 ℃, and then 50 nM LTG was added and incubated for 20 min. 50 μg/mL rapamycin was applied to the cells to induce mitophagy. The fluorescence images were recorded at different time points, such as 0, 40 and 80 min.

For real-time mitophagy tracking and co-localization video of **BYM** with LTG, 0.25 μM **BYM** was added to the culture dish and incubated for 15 min at 37 ℃, and then 50 nM LTG was added and incubated for 20 min. 100 μg/mL rapamycin was applied to the cells to induce mitophagy. Cell images were taken every 3 seconds in the period of 40 min.

The digital images were recorded on a Carl Zeiss LSM 800 super high resolution laser confocal microscope. The excitation wavelength was set at 405 nm for Hoechst 33342 or MitoLite^{TM}-blue, 488 nm for LTG or LC3 protein and 561 nm for **BYM** and Mito-Tracker Red CMXRos, respectively.

2.8 MTT assay

MTT assays were performed to evaluate the cell toxicity of the compounds. The human cervical cancer cells (HeLa), human prostate cancer cells (PC3) and human bronchial epithelioid noncancerous cells (16HBE) were examined. The cells were cultured in the 96-well plates with a density of $4x10^4$ cells/mL and grown in an incubator at 37 °C with 5% CO_2 for 24 h, then were treated with the compound at the concentration of 40, 30, 20, 10, 5, 2.5, 1.25 and 0 μM, respectively. After incubation for 48 h, the medium containing the compound was discarded and 0.5 mg/mL MTT solution was added for further incubation 4 h in dark. After that, the MTT solution was discarded and DMSO was added to ensure the deck adhering to 96-well plate complete dissolution. The optical density (OD) was measured by using a microplate reader (Thermo Fisher) and the absorption wavelength was 570 nm. Finally, the cell survival rate and the half-maximal inhibitory

concentration (IC_{50}) of compounds on the cells were calculated from the OD values.

2.9 CsA Pre-treatment for HeLa cells and cell imaging

For this experiment, HeLa cells were cultured in confocal dishes for 24 h and then treated with 2.5 μM Cyclosporin A (CsA, Sigma, USA) for 24 h to block the mitochondria inner membrane permeability transition pore. After that, 5 μM **BYM** was added to incubate with cells for 30 min.

2.10 Flow cytometry analysis

In the flow cytometry experiments, HeLa cells were cultured in a 6-well plate for 24 h and then treated with 1 μL DMSO for 80 min (control), 50 μg/mL rapamycin for 80 min and 100 μg/mL rapamycin for 40 min, respectively. After that, cells were washed twice with PBS and digested by trypsin (free EDTA). After collecting and centrifuging the cells, 195 μL of 1× Annexin V binding buffer was added for resuspension, then 5 μL of Annexin V-PE was added for staining for 10 min. The sample acquisition was performed using a flow cytometer (BD Biosciences). The data were analyzed via FlowJo software.

3. Results and discussion

3.1 Molecule design of new benzo-indole and indole styryl conjugates as turn-on fluorescent probes

Four new mitochondria-specific fluorescent probes **BYM**, **YM**, **BYP** and **YP** were synthesized by a straightforward two-step reaction with good yields (**Scheme S1**). All compounds were characterized with ^{1}H NMR, ^{13}C NMR, and high resolution mass spectroscopy (HRMS). The characterizations were shown in **Figure S1-S4** in Supporting Information. In the molecular design of the probes targeting mitochondria, a rigid and planar scaffold of benzo-indole or indole was integrated with a *p*-substituted styrene group (4-morpholinyl and 4-methylpiperazin-1-yl), which possesses hydrogen bond acceptor sites (oxygen and nitrogen atoms) to enhance interaction affinity with substrates. The two molecular fragments were connected via a flexible and rotatable ethylene bridge to generate a π-conjugated system. The free ligand in solution shows almost no fluorescence signal. When the viscosity of the medium is increased, the free rotation of the probe is restricted and thus it emits strong fluorescence signal (**Figure S5**) due to the non-radiative decay pathway is suppressed.[49, 50] This fluorescent “turn-on” mechanism may provide a useful chemical sensing tool for the study of ligand interaction targeting G-quadruplex structures in vitro and in live cells.

3.2 Spectroscopic property of the fluorescent probes and their interaction property with nucleic acids

The spectral data of the probes were summarized in **Table 1**. A comparison of the property of some fluorescent probes reported recently in sensing of various mitochondrial G4-DNA substrates *in vitro* was given in **Table 2**. The maximum absorption peaks of the probes are in the visible region (484-505 nm) and red-shifted absorption is generally observed in non-polar solvent **(Figure S6)**. The emission wavelength is in the range of 576-615 nm upon excitation (**Figure S7**). As shown in **Figure 1**, the probes show only weak fluorescence in the Tris-HCl buffer. Fluorescence and UV-vis titration experiments were performed to study the interaction property and binding preference of the probes with mtG4-DNA and other type of nucleic acids (**Figure S8-S12**). Upon the addition of nucleic acid substrates including ssDNA, dsDNA, mitochondrial double-stranded DNA (mt-dsDNA) and mitochondrial G4-DNA (mtG4-DNA), the probes were able to induce intensive interaction signal (λ_{em} in the range of 570-620 nm) for most mtG4-DNA substrates, while the interaction signal with ssDNA, dsDNA and mt-dsDNA was found generally much weaker. In addition, a red shift at the absorption maxima of the probe in the visible region was generally observed upon binding to the mtG4-DNA substrates while it was not appeared with ssDNA, dsDNA and mt-dsDNA. The results indicate that these probes may have high selectivity towards the mtG4-DNA over other type of nucleic acids. Furthermore, among the four fluorescent probes, **BYM** and **YM**, both bearing a 4-morpholinostyryl group, generated much stronger interaction signal towards the ten mtG4-DNA substrates selected from difference regions of the human mitochondrial gene. For **BYM**, it induces remarkably intensive interaction signal upon binding to mt16250 (19-fold enhancement) and mt6363 (28-fold enhancement).

Table 1. The spectroscopic properties of the mitochondrial-specific fluorescent probe.[a]

Probe [b]	$\lambda_{Abs,\,max}$ (nm)	$\varepsilon_{Abs,\,max}$ ($M^{-1}cm^{-1}$) [c]	λ_{ex} (nm)	λ_{em} (nm)	**Stokes shift** [d]	**Φf** [e]
BYM	505	34000	530	615	85	0.389
YM	497	36000	540	597	57	0.093
BYP	494	20667	524	598	74	0.275
YP	484	16000	510	576	66	0.090

[a] Experiments were performed in 10 mM Tris−HCl buffer at pH = 7.4.
[b] The concentration of the probe used was 0.5 μM.
[c] Molar extinction coefficient (ε) at the absorption maxima (nm) of the ligand in visible region.

[d] Stokes shift.

[e] Relative fluorescence quantum yield of probes was estimated upon the addition of 0.67 μM mt6363. The standard of the relative fluorescence quantum yield is fluorescein ($\Phi_f = 0.95$, methanol with 1% NaOH). Fluorescence quantum yield was tested on a Fluorolog-3 spectrofluorometer produced by HORIBA Instruments Incorporated.

Table 2. A comparison of the performance of fluorescent probes in sensing of various mitochondrial G4-DNA substrates *in vitro*.

Probe	λ_{ex} (nm)	λ_{em} (nm)	Stokes shift (nm)	LOD (nM)	Φf	Ref.
***o*-BMVC-12C-P**	470	~580	110	-	0.55-0.75	[31]
DMOTY	430	520	90	-	0.284-0.506	[42]
NCT	466	650	184	3.1-8.7	0.022	[35]
IZIN-1	538	660	122	-	-	[36]
TPE-mTO	488	530-540	42-52	4.1	-	[51]
DMOTY& SCY-4	440/564	510/581	70/17	-	0.028-0.102	[44]
BYM	505	615	85	1.52	0.389	This work

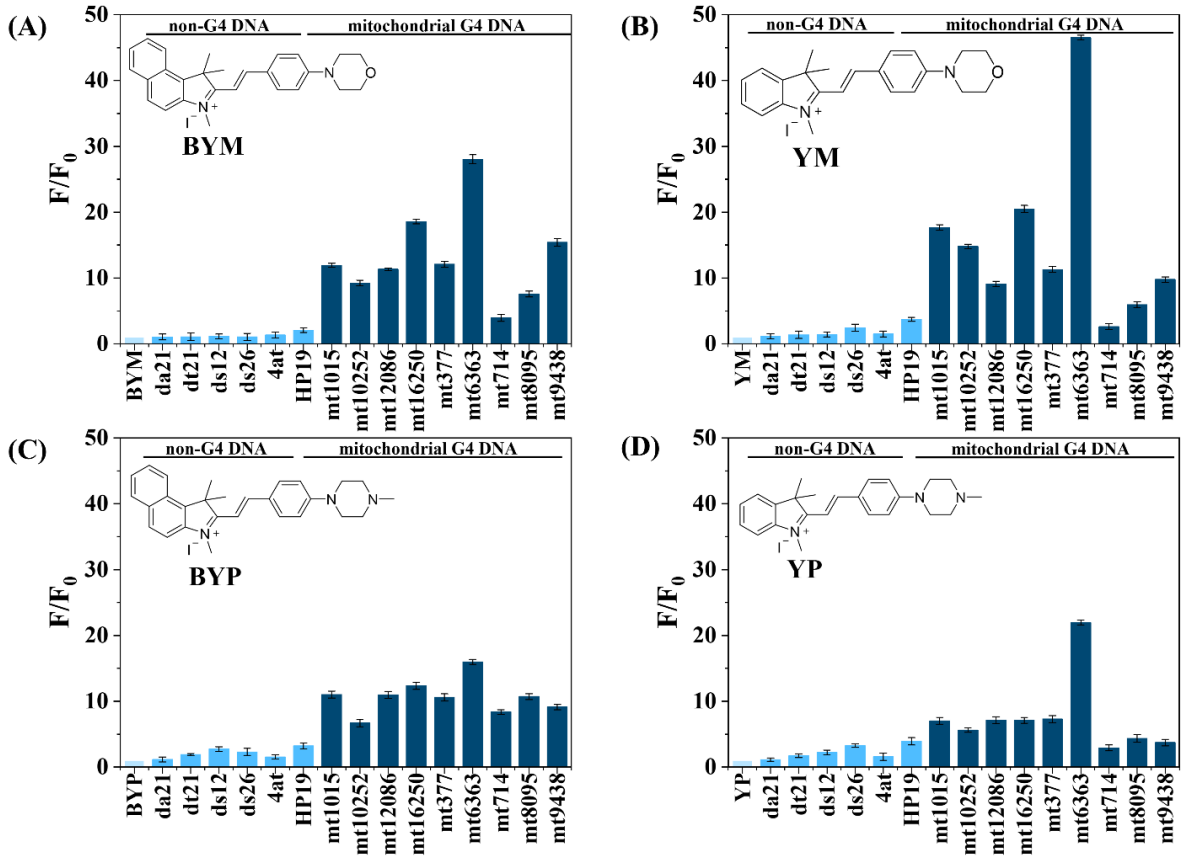

Figure 1. (A-D) The fluorescence intensity induced upon the probes (**BYM**, **YM**, **BYP**, and **YP**) binding to different DNA substrates. Single-stranded DNA: da21, dt21; duplex DNA: ds12, ds26, 4at; mitochondrial duplex DNA: HP19; mitochondrial G4-DNA: mt1015, mt10252, mt12086, mt16250, mt377, mt6363, mt714, mt8095, mt9438. The concentration of the probes was 0.5 μM in a 10 mM Tris-HCl buffer containing 60 mM KCl. The concentration of DNA substrates was used at the maximum of the fluorescent signal enhancement (3.4 μM).

3.3 Sensitivity and selectivity of BYM towards mitochondrial DNA G-quadruplexes

From the fluorescence titration experiments, the equilibrium binding constant (K_{eq}), linear region and limit of detection of the probes towards various mtG4-DNA substrates were estimated. The results were summarized in **Table S2** for comparison. The two merit probes, **BYM** and **YM**, generally exhibited good linear response range and limit of detection (LOD, down to 1.52 nM) to the mtG4-DNA substrates, in particular mt6363 showing high binding affinity (K_{eq} in the range of 7.5×10^6 - 10.8×10^6 M^{-1}) with the probes (**Figure 2**). The influence of pH conditions for the probe interacting with mt6363 was investigated and the results (**Figure S13**) showed that the strong fluorescent interaction signals were markedly observed under the pH conditions 3 to 10. Moreover, some common cellular sulfhydryl compounds including GSH, HSO_3^- and H_2S did not show significant interference on the fluorescence emission of probes (**Figure S14**). The results demonstrate that the probe could be developed as a mitochondria-specific fluorescent probe targeting the mtG4-DNA substrates under in vitro and intracellular conditions.

To demonstrate further the specific binding of **BYM** to mitochondrial G4-DNA against the single-/double-stranded DNA substrates *in vitro*, competition studies were conducted (**Figure 3**). In the competition experiments, the substrates of ssDNA (dt21), dsDNA (ds26) and mt-dsDNA (HP19) were applied to compete with mt6363 in buffer solution. The results show that only a very small reduction of fluorescent signal was observed with the addition of excessive competing substrates (at 10-fold molar equivalents to mt6363), which may evidently indicate that **BYM** has a much stronger binding affinity with the mtG4-DNA mt6363 (**Figure 3A-C**). In addition, to demonstrate the target of probe is G4-structure favorable, a well-known G4-specific binding ligand BRACO-19 was utilized to compete with mt6363 (**Figure 3D**). It was found that the addition of BRACO-19, from 1-8 molar equivalents of **BYM** to compete with mt6363 in buffer solution, the fluorescence signal intensity was decreased gradually, which may indicate that both **BYM** and BRACO-19 are preferentially binding to G4-substrates. Furthermore, the binding stoichiometry for **BYM**–mtG4-DNA complex determined with Job plot analysis is 1:1 (**Figure 3E-F**).

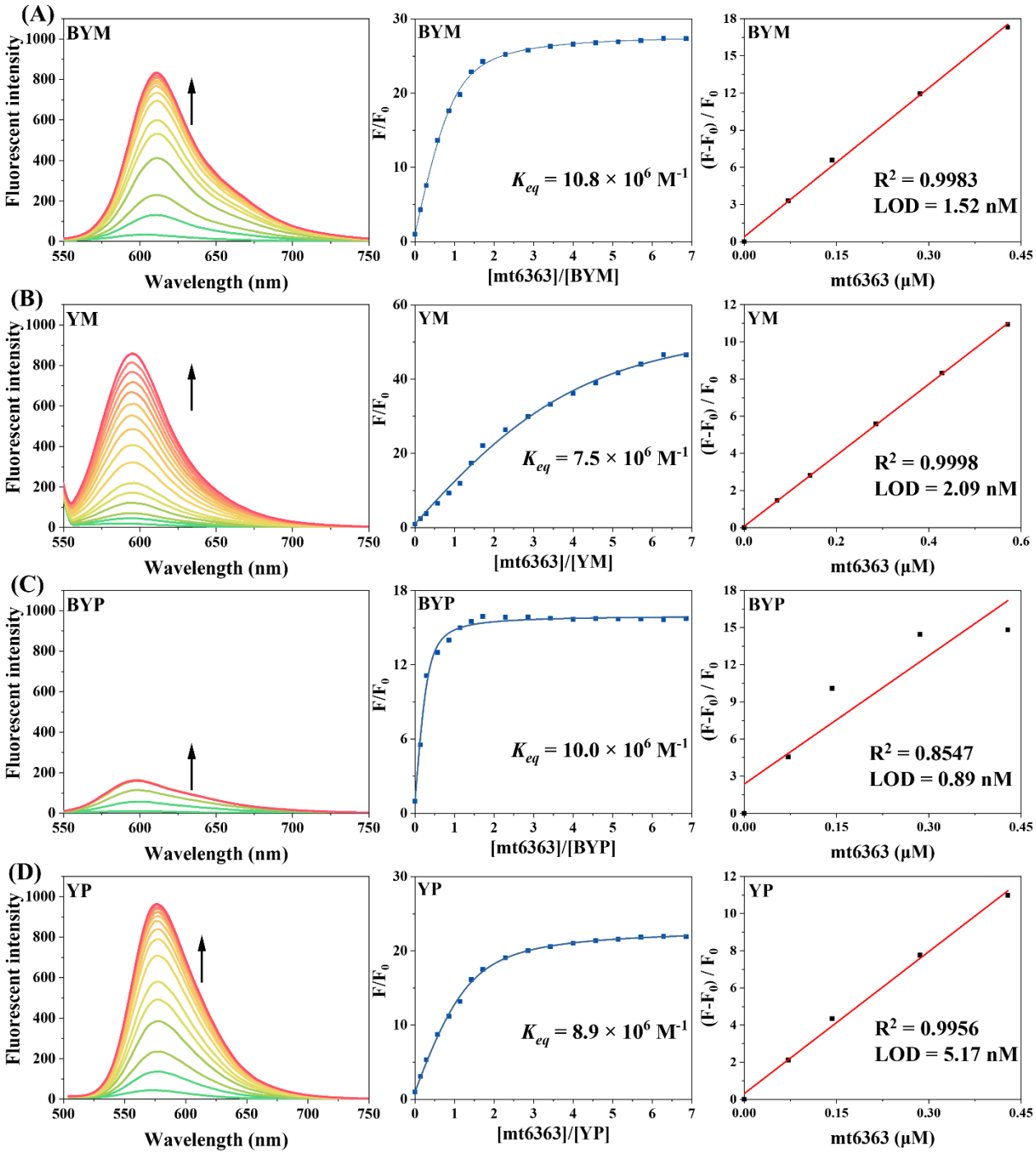

Figure 2. Fluorescence titration spectra of probes (0.5 μM) with mt6363 (0-3.4 μM) and their equilibrium binding constants, linear response range and limit of detection. (A) **BYM**; (B) **YM**; (C) **BYP**; (D) **YP**.

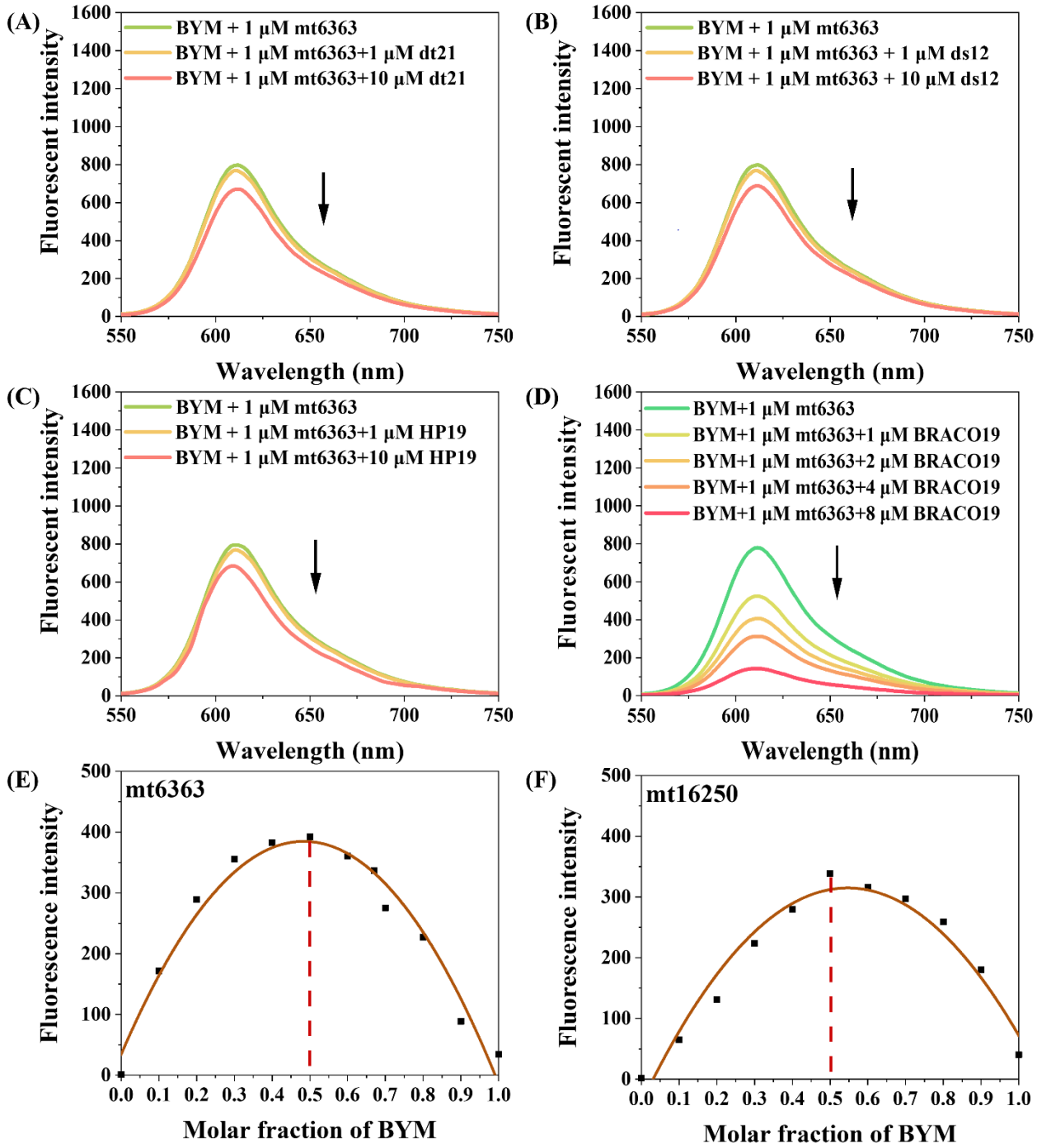

Figure 3. Competition study of **BYM** between mt6363 G4-DNA and other nucleic acids: (A) mt6363 at 1 μM and dt21 was added at the concentrations 1 μM and 10 μM; (B) mt6363 at 1 μM and ds26 was added at the concentrations 1 μM and 10 μM; (C) mt6363 at 1 μM and HP19 was added at the concentrations 1 μM and 10 μM; (D) mt6363 at 1 μM and BRACO-19 was added at the concentrations 1 μM, 2 μM, 4 μM and 8μM. The concentration of **BYM** was 0.5 μM in Tris−HCl buffer (10 mM, pH 7.4) containing 60 mM KCl. (E) Job plot analysis of the binding stoichiometry of **BYM** and mt6363; (F) Job plot analysis of the binding stoichiometry of **BYM** and mt16250.

The fluorescence lifetime of **BYM** and its complexes with various types of DNA substrates in Tris-HCl buffer was studied (**Figure 4** and **Figure S15-S19**). The free ligand exhibits a rapid decay with a lifetime of 0.06 ns in the buffer solution. After binding to the single-/double-stranded DNA substrates that have weak binding affinity with the probe, the lifetime was found only slightly increased (0.07-0.11 ns). Interestingly, when the probe interacts with mtG4-structures including mt10252 (0.69 ns), mt12086 (0.58 ns), mt6363 (1.16 ns) and mt9438 (0.6 ns), the fluorescence lifetime was remarkably increased in the range of 0.17-1.16 ns. The result could be probably due to the strong interaction of the probe with the G4-structure effectively limiting the free rotation of the molecule in solution.

The influence of **BYM** on the mtG4-DNA topology was investigated with circular dichroism (CD) analysis. The mtG4-DNA substrates (**Figure S20**: mt6363 (parallel conformation), mt16250 (parallel conformation) and mt12086 (hybrid conformation)) showing strong binding affinity with **BYM** were selected for study. From the CD spectra (**Figure S21**), it shows that the interaction of the probe did not cause significant conformation change to the mtG4-structure. In addition, as indicated from the CD melting study (**Figure S22**), an increased melting temperature (ΔT_m = 5 °C) for **BYM**-mt6363 complex was observed and it may support that the ligand could be able to stabilize the mtG4-DNA structure.

It has been demonstrated that the binding modes of hemin take place at terminal regions of G4s *via* end-stacking.[52, 53] To investigate whether our new mitochondrial probes interact with the mt-G4-DNA through the end-stacking mode similar to that of hemin, the competition assays with hemin were conducted. As shown in **Figure S23**, when hemin at 1 μM (or 10 μM) was added to the solution to compete the binding sites of mt6363 G4-DNA that the probe occupied (intensive interaction fluorescent generated), the fluorescence intensity was markedly decreased, indicating that hemin may replace the binding sites occupied by the probe. Therefore, the results suggest that the probes may probably interact with the G4-structures *via* end-stacking modes.

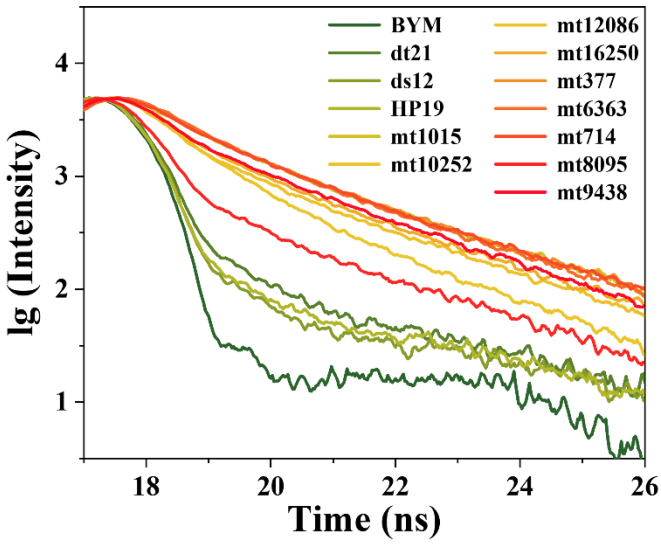

Substrate	lifetime (ns)
BYM	0.06
BYM-dt21	0.07
BYM-ds12	0.11
BYM-HP19	0.07
BYM-mt1015	1.06
BYM-mt10252	0.69
BYM-mt12086	0.58
BYM-mt16250	0.76
BYM-mt377	1.09
BYM-mt714	1.06
BYM-mt6363	1.16
BYM-mt8095	0.17
BYM-mt9438	0.60

Figure 4. The fluorescence lifetimes of **BYM** and its DNA complexes in a 10 mM Tris-HCl buffer containing 60 mM KCl at pH 7.4 at room temperature.

3.4 Cytotoxicity of BYM and the visualization of mitochondrial G4-DNA in HeLa cells

To be a good sensor for intracellular monitoring and live cell imaging of target substrates, the probe with minimum disruption of cellular functions or non-toxic to the live cells is highly important. We thus conducted MTT assays to evaluate the acute toxicity of probes to a number of human cell lines. The results (**Figure S24** and **Table S3**) show that the probes were not very toxic against HeLa, PC3 and 16HBE cells after incubated for 48 h. The IC_{50} values of **BYM** and **YM** were found in the range of 16-37 μM and 71-106 μM, respectively. For the treatment with **BYM** and **YM** at 5 μM, the survival rate of all these cells was higher than 90%, which indicate that the probe under this concentration may be non-toxic to the cells and is suitable for live cell imaging and intracellular monitoring of mtG4-DNA. In addition, we found that HeLa cells treated with **BYM** at 5 μM did not significantly induce mitochondrial ROS production (**Figure S26**), which is different from most of mtG4-DNA probes that cause mitochondrial dysfunction and increase ROS level in the mitochondria.[31, 54]

As indicated from **Figure S25**, **BYM** is able to stain selectively the mtG4-DNA bands including mt10252, mt16250 and mt6363 in the polyacrylamide gel electrophoresis (PAGE), while ssDNA and dsDNA bands were almost invisible. Its staining performance is better than the commercial probe SYBR Gold, which has low substrate selectivity and low staining signal under same concentration. **BYM** was then applied in cell imaging experiments (**Figure 5**). It was found

BYM is a mitochondria-specific probe and it only stains the cytoplasm but not the nucleus where clearly stained by Hoechst 33342 (**Figure 5A**). To demonstrate the target stained by **BYM** is mitochondria but not lysosomes in cytoplasm, the co-localization study with MitoLite^{TM}-Blue (a mitochondria-specific probe) and Lyso-Tracker Green (LTG, a lysosome-specific probe) were conducted. From the merged confocal images, **BYM** is highly overlapped with MitoLite^{TM}-Blue (**Figure 5B**); however, it was almost no co-localization with lysosomes (**Figure 5C**). The Pearson's co-localization coefficient, which describes the correlation of the distribution of the two channels, calculated by Image-Pro Plus was 0.88. The results indicate that the cellular organelle **BYM** located is mitochondria and the fluorescence signal is attributed from the interaction of the probe with mtG4-DNA structures in the mitochondria. Despite **BYM** does not enter the nucleus, it also shows strong interaction signal with the G4-DNA of telomere and promoter located in nucleus (**Figure S27**) because the probe is highly selective binding to G4-DNA structures *in vitro* and in cellular. In addition, the probe generally shows certain degree of binding preference towards the parallel G4-strucutre compared to anti-parallel and hybrid topologies (**Figure S28**).

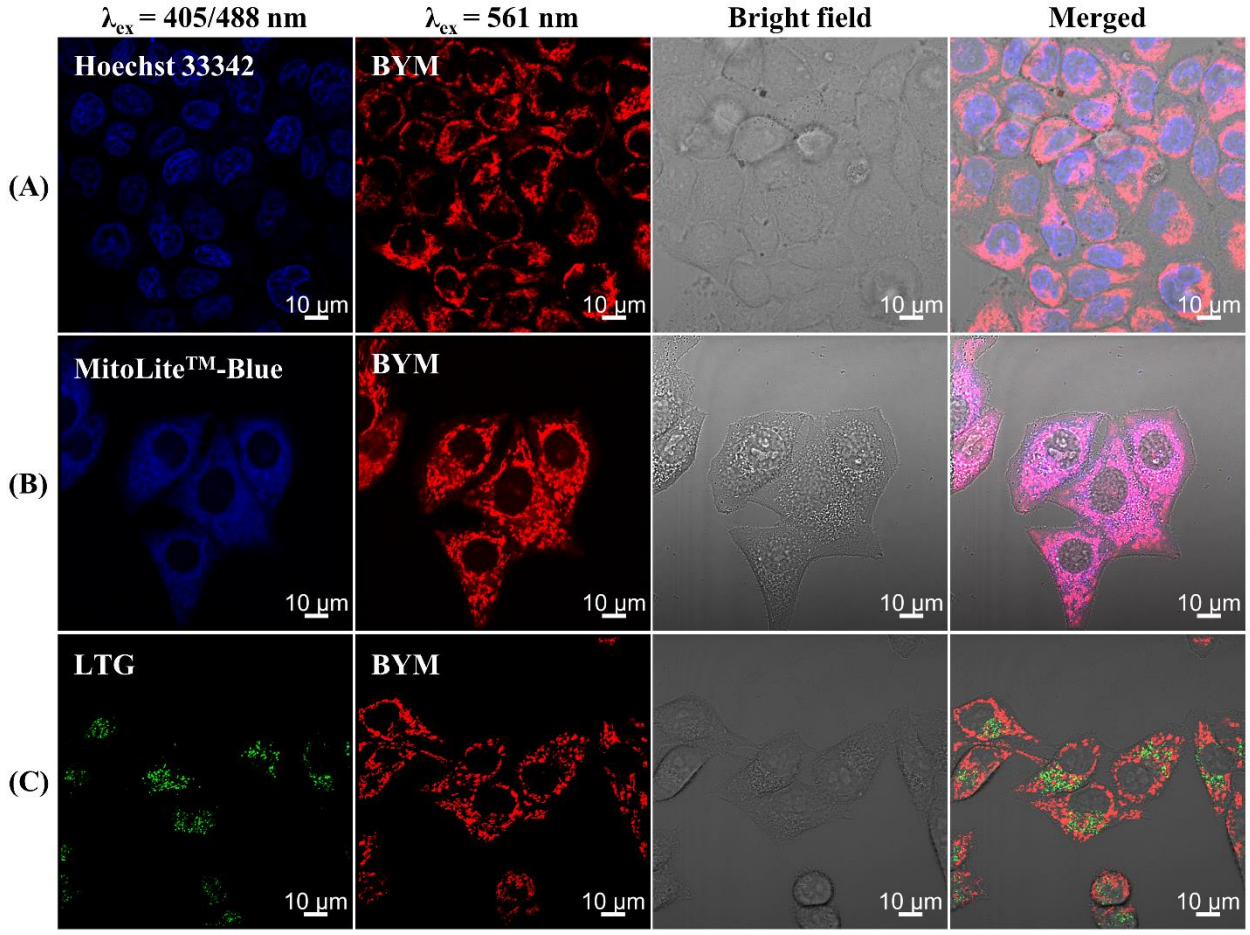

Figure 5. (A) Staining of HeLa cells with 5 μM **BYM** for 30 min and 1 μg/mL Hoechst 33342 for

20 min; (B) Staining of HeLa cells with MitoLite^{TM}-Blue for 1 h and 5 μM **BYM** for 30 min; (C) Staining of HeLa cells with 5 μM **BYM** for 30 min and 50 nM Lyso-Tracker Green (LTG) for 20 min. The scale bar is 10 μm.

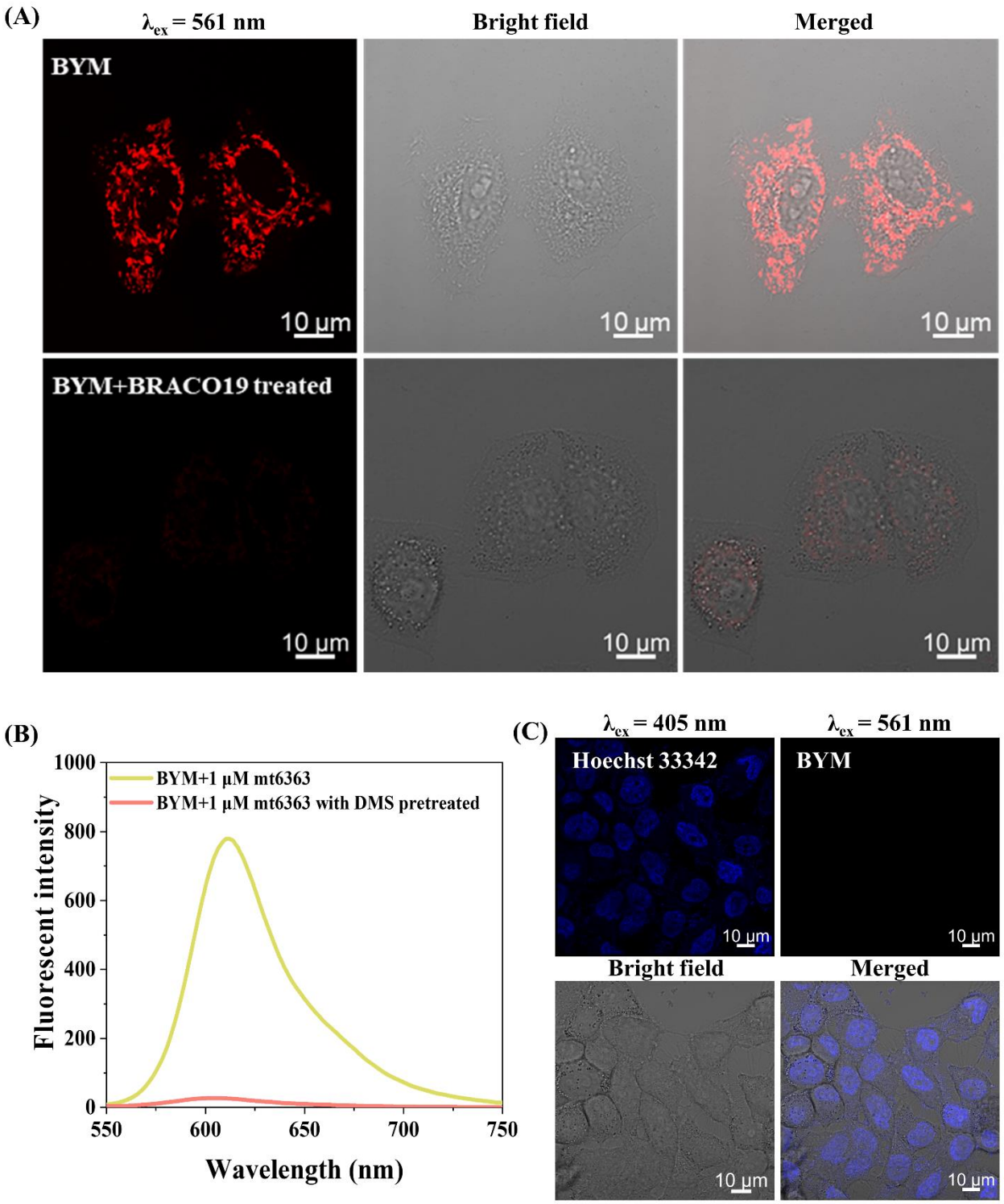

Figure 6. (A) Fluorescence images of HeLa cells stained with 5 μM **BYM** for 30 min and 8 μM BRACO-19 for 30 min. (B) Fluorescence intensity of **BYM** and 1 μM mt6363, **BYM** and 1 μM mt6363 with **DMS** pretreated; (C) Fluorescence images of HeLa cells treated with 20 mM dimethyl sulfate (DMS) for 20 min, 5 μM **BYM** for 30 min and 1 μg/mL Hoechst 33342 for 20 min. The scale bar is 10 μm.

The DNase and RNase digestion assays (**Figure S29**) were performed to conform the binding substrates of **BYM** in the mitochondria are DNA but not RNA. The results show that the fluorescence signal in the cells was completely disappeared after the DNase treatment while RNase treatment did not cause observable changes to the fluorescent stains. The results indicate that the substrates interacted with **BYM** in mitochondria were mostly DNA. To demonstrate further these mitochondrial DNA substrate interacted with **BYM** most likely were G4-structures, intracellular competitive experiments with BRACO-19 (a non-emissive and G4-specific ligand) were performed (**Figure 6A**). We found that the red fluorescence signal of **BYM** in the cytoplasm was almost disappeared after the addition of BRACO-19, indicating that **BYM** and BRACO-19 may have similar cellular targets and presumably are G4-structures. Furthermore, to obtain more evidence to support further the binding substrates of **BYM** in mitochondria is G4-DNA, the live HeLa cells were exposure to dimethyl sulfate (DMS), which is able to methylate the N7 atoms of guanines in single-/double-stranded DNA substrates and thus it prevents the DNA from forming G4-structures in the cells. After DMS pretreatment, **Figure 6B-C** indicates that the red fluorescence intensity of the cell staining was almost completely disappeared due to loss of G4 substrates for interaction with **BYM** in mitochondria, while the Hoechst 33342 dye (blue emission) was not affected. **BYM** may be a useful probe for mapping G4-structures in the mitochondria of live cells.

Fluorescent probes with high stability against photobleaching are highly desirable for live cell imaging and intracellular monitoring of biomolecules. We thus tested the photostability of **BYM** in solution and in live HeLa cells. For the solution with **BYM** interacted with mtG4-DNA (**Figure S30**) irradiated under λ_{ex} = 530 nm for 50 min, the fluorescence signal intensity was just slightly decrease and over 92% of the intensity was retained. For live cell experiment, under the irradiation (λ_{ex} = 561 nm), cell images were taken every 3 seconds in the period of 50 min. At the first 100 scans, the fluorescence intensity showed no observable decrease. For 200-300 scans, the intensity of the stain in the cells was obviously reduced but was still observable by naked eye. After 500 scans, the fluorescence stain in the cells became every weak and the intensity remained was about 34% of the original (**Figure S31A** and the real-time video record attached). Furthermore, the photostability of the probe was compared with a commercial mitochondrial dye (Mito-Tracker Red CMXRos) in HeLa cells under the same conditions (**Figure S31B**). It was found that the cellular fluorescent signal of Mito-Tracker Red CMXRos mostly faded away after 200 scans while that of **BYM** was still clearly observable. The results support that **BYM** is robust against photobleaching.

3.5 Real-time visualization of mitophagy with BYM in live Hela cells

The delivery of **BYM** probe is different from most of the commercial mitochondrial probes that are based on the electrostatic-attraction of the cationic dye and mainly via the mitochondrial membrane potential (MMP) such as Rho123, JC-1 and tetraphenylphosphonium (TPP^+).[20, 55, 56] We thus conducted experiments to demonstrate the staining of mitochondria with **BYM** was not depending on MMP. Rho123, which is a commercial and electrostatic-attraction based cationic mitochondrial probe, was used as a control in the experiments. The protonophore, carbonylcyanide 3-chlorophenylhydrazone (CCCP), was applied to decrease the MMP. As shown in **Figure 7**, HeLa cells after treating with 10 μM CCCP for 20 min, the intensity of the red fluorescence stain (**BYM**) in the cells showed no significant changes while the fluorescence of Rho123 was disappeared completely. In addition, the cells after fixed with 4% polyformaldehyde, the MMP was vanished; however, the strong and red fluorescent staining of **BYM** was retained because the probe is selectively bound to the mtG4-DNA in the mitochondria. We then preformed cyclosporin (CsA) assays in HeLa cells to block the permeability transition pore (PTP) on the mitochondrial inner membrane. From the cell images shown in **Figure S32**, it was found that the cells without treated with CsA, intensive fluorescent signal was observed; however, after CsA pre-treatment, almost no staining was observed. The results indicate that **BYM** may pass through the permeability transition pores and then interacts with mtG4-DNA substrates in mitochondria to generate fluorescence signal.

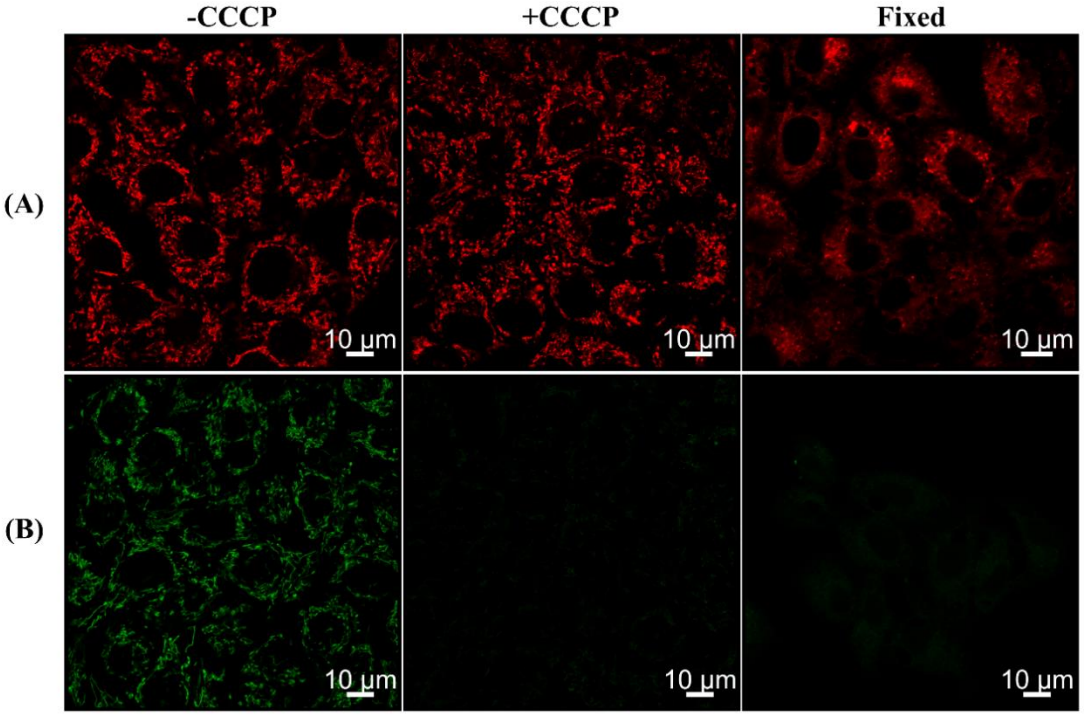

Figure 7. (A) HeLa cells treated with 5 μM **BYM** for 30 min and then treated with CCCP (middle),

without CCCP (left) or 4% polyformaldehyde (right); (B) HeLa cells treated with 1 μM Rho123 for 30 min and then treated with CCCP (middle), without CCCP (left) or 4% polyformaldehyde (right). The scale bar is 10 μm.

To further confirm the cellular location of **BYM**, we used **BYM** and Lyso-Tracker Green (LTG, a commercial probe for lysosome labeling) to co-stain HeLa cells under the conditions with or without rapamycin pre-treatment. Rapamycin is a typical autophagy inducer.[57] The HeLa cells after treated with 50 μg/mL rapamycin, mitophagy (mitochondrial autophagy) was found increased as the green foci (LTG stain) was gradually increased (**Figure 8**). In addition, the stains of **BYM** and LTG were well co-localized in the mitochondria as indicated from the Pearson's correlation increased from 0.17 (at 0 min) to 0.23 at 40 min and 0.4 at 80 min, respectively. In addition, from **Figure 8**, it is noteworthy that the fluorescence intensity of **BYM** at the location overlapped with LTG stains was increased gradually as mitophagy was enhanced from 0 to 80 min. It could be probably due to the accumulation of the emissive **BYM**-mtG4-DNA complexes in the lysosome. Therefore, **BYM** could be a potential biosensor for real-time visualization of mitophagy in live cells. In the control experiment (**Figure S33**) without rapamycin to induce mitophagy, this interesting appearance was not observed and the Pearson's correlation only showed minor variations. Taken together the results obtained, it may support that the new probe **BYM** is mitochondria-specific and the binding target most likely is mtG4-DNA.

The immunofluorescent colocalization of the autophagosome protein LC3 and **BYM** in HeLa cells was investigated. As shown in **Figure 9**, HeLa cells were exposed to 50 μg/mL rapamycin for 0 min, 40 min, 80 min respectively to induce mitophagy and then were co-stained with **BYM** and LC3 antibody. The merged confocal image and Pearson's correlation for the immunofluorescent colocalization (**Figure 9D**) showed that the immunofluorescence of LC3 (green) and **BYM** (red) was well co-localized in the cells. Furthermore, our control studies shown in **Figure S34** indicated that the addition of rapamycin at 50 μg/mL for 80 min or at 100 μg/mL for 40 min in HeLa cells did not cause significant apoptotic cell death (cell viability maintained > 95%) despite mitophagy was markedly observed in the cells under these conditions.

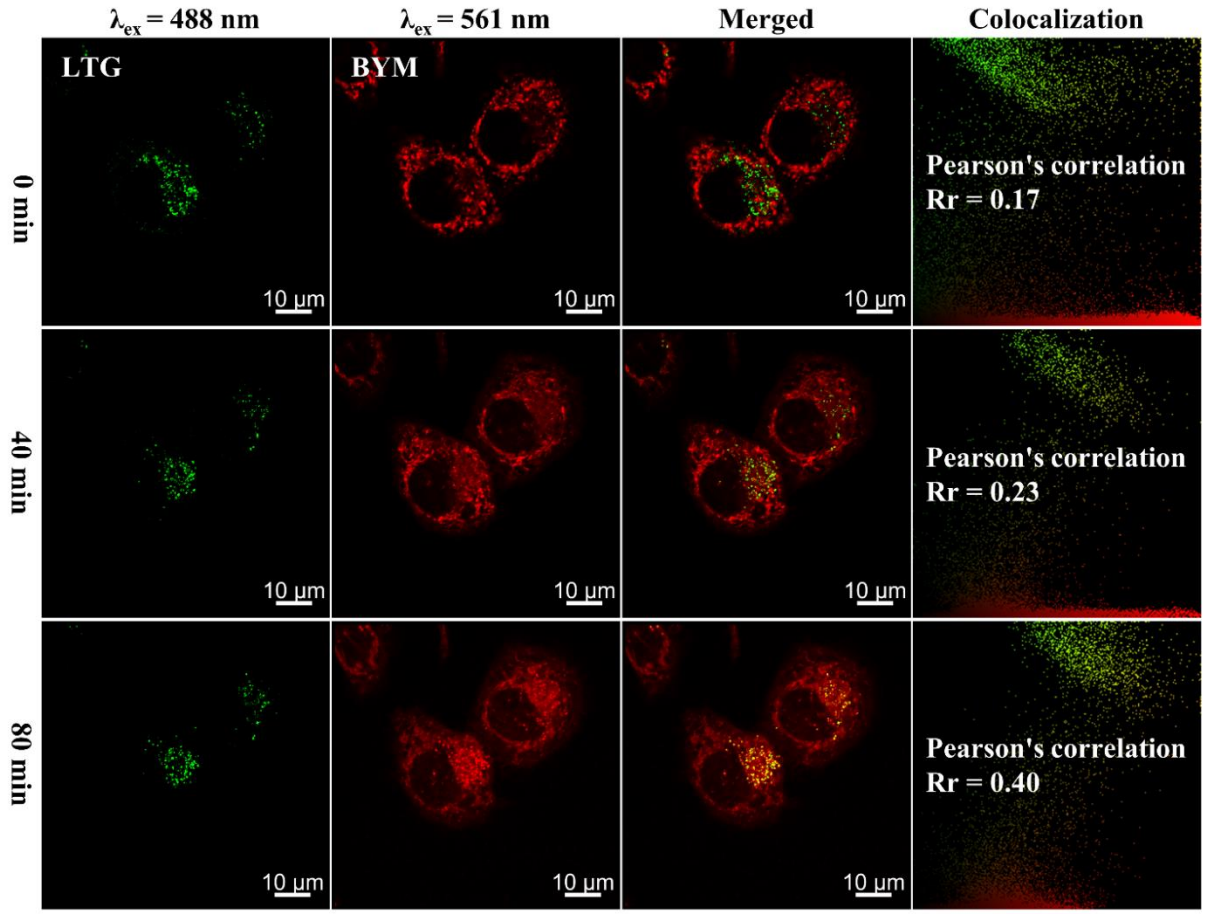

Figure 8. Confocal images for the co-localization analysis. HeLa cells were treated with 50 μg/mL rapamycin and co-stained with **BYM** (5 μM) and LTG (50 nM) from 0 to 80 min. The scale bar is 10 μm.

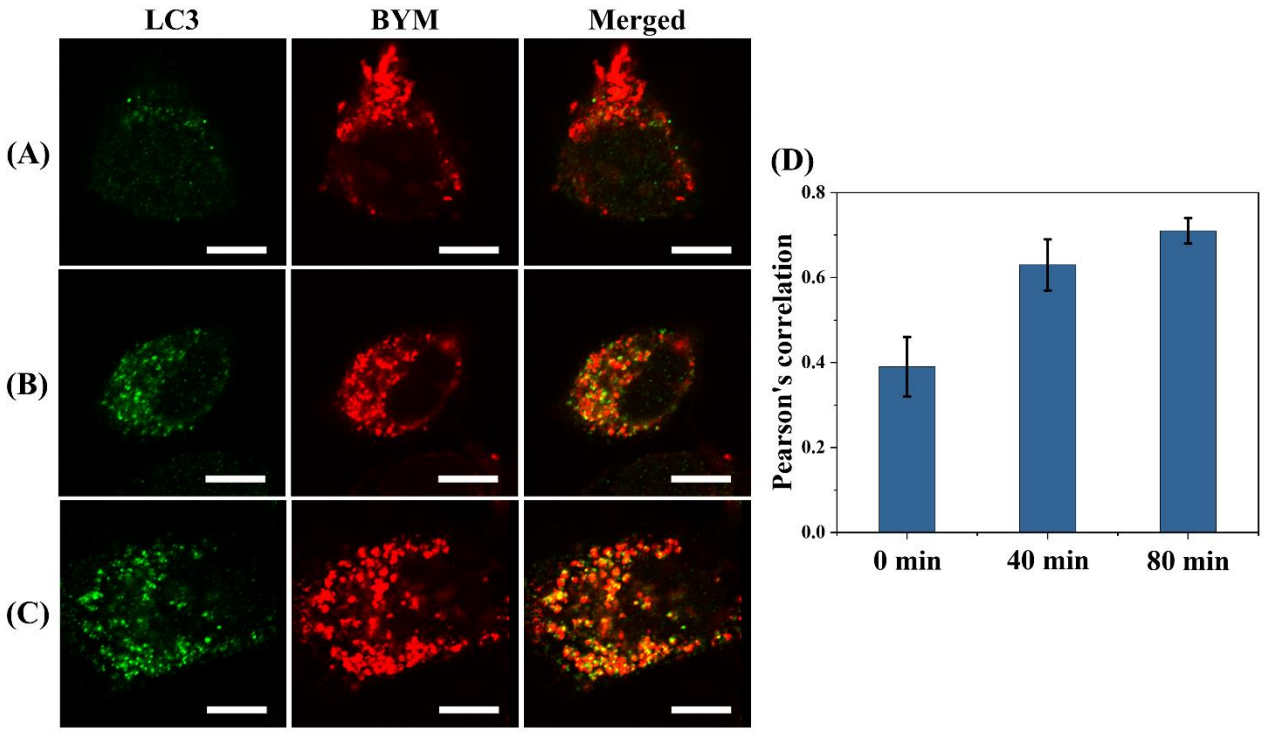

Figure 9. Immunofluorescent colocalization of autophagosome protein LC3 (green) and **BYM** in HeLa cells. HeLa cells were exposed to 50 μg/mL rapamycin for 0 min, 40 min, 80 min to induce

mitophagy. (A) 0 min; (B) 40 min; (C) 80 min; (D) Pearson's correlation for the immunofluorescent colocalization of LC3 (green) and **BYM** in HeLa cells. Pearson's correlation per condition is presented as means ± SEM. About 5~20 cells per condition were counted. The scale bar is 10 μm.

4. Conclusion

In conclusion, a series of new mitochondrial G4-DNA probe was synthesized based on the integration of the small and planar molecular scaffolds of benzo-indole/indole with a *p*-substituted styrene moiety. Cell imaging study showed that the ligands were targeting mitochondria selectively but not entering the nucleus. Fluorescence and UV-vis titrations and competition experiments showed that one of the ligands, **BYM**, exhibits high selectivity interacting with mitochondrial G4-DNA while the binding affinity towards other non-G4 nucleic acid structures including single-/double-stranded DNA and hairpin was found very lower. The equilibrium binding constant of **BYM** for mitochondrial G4-DNA determined is almost 1000-fold higher than that of mitochondrial double-stranded DNA. The ligand was found showing low cytotoxicity against a number of human cancer and noncancerous cells, which may indicate that **BYM** is a merit ligand targeting-mitochondrial G4-DNA structures for bioorthogonal study in live cells. In addition, the delivery of **BYM** to mitochondria is not mitochondrial membrane potential dependent but mainly through the permeability transition pore on the mitochondrial inner membrane. The probe was also successfully demonstrated in the monitoring the dynamic process of mitochondrial autophagy. Taken together, **BYM** has excellent stability against photobleaching and high selectivity and sensitivity targeting mitochondrial G-quadruplexes. It may provide a sensitive, selective and low cytotoxicity fluorescent tool for real-time study of mitochondrial functions in live cells.

ACKNOWLEDGMENT

We would like to thank Dr. Xiao Zhou and Dr. Hang Bai from the Analysis and Test Center, Guangdong University of Technology for their assistance in cell imaging experiments.

FUNDING

This work was supported by the National Natural Science Foundation of China [81473082, 22077020 and 32050410289], Natural Science Foundation of Guangdong Province, China [2017A030313078, 2017A030313071, and 2019A1515011799], Department of Education of Guangdong Province, China [2016KCXTD005 and 2017KSYS010], Department of Agriculture

and Rural Affairs of Guangdong Province, China [2018LM2175], Health and Medical Research Fund (HMRF), Hong Kong SAR [19200231], PolyU Startup Fund [P0035712], PolyU SZRI fund [A0039278], and Special Funds for the Cultivation of Guangdong College Students' Scientific and Technological Innovation [pdjh2020a0175].

Conflict of interest statement. The authors declare no conflicts of interest.

Reference

[1] M. Xia, Y. Zhang, K. Jin, Z. Lu, Z. Zeng, W. Xiong, Communication between mitochondria and other organelles: a brand-new perspective on mitochondria in cancer, Cell & Bioscience 9(1) (2019) 27-45. https://doi.org/10.1186/s13578-019-0289-8.

[2] B. Westermann, Mitochondrial fusion and fission in cell life and death, Nature Reviews Molecular Cell Biology 11(12) (2010) 872-884. https://doi.org/10.1038/nrm3013.

[3] R. Horbay, R. Bilyy, Mitochondrial dynamics during cell cycling, Apoptosis 21(12) (2016) 1327-1335. https://doi.org/10.1007/s10495-016-1295-5.

[4] V. Roca-Agujetas, C.d. Dios, L. Lestón, M. Marí, A. Morales, A. Colell, Recent Insights into the Mitochondrial Role in Autophagy and Its Regulation by Oxidative Stress, Oxidative Medicine and Cellular Longevity 2019 (2019) 3809308. https://doi.org/10.1155/2019/3809308.

[5] Y. Liu, L. Teng, L. Chen, H. Ma, H.-W. Liu, X.-B. Zhang, Engineering of a near-infrared fluorescent probe for real-time simultaneous visualization of intracellular hypoxia and induced mitophagy, Chemical Science 9(24) (2018) 5347-5353. https://doi.org/10.1039/C8SC01684D.

[6] J. Sarparanta, Garcia-Macia, Marina, R. Singh, Autophagy and Mitochondria in Obesity and Type 2 Diabetes, Current Diabetes Reviews 13(4) (2017) 352-369. https://doi.org/10.2174/1573399812666160217122530.

[7] W. Wang, F. Zhao, X. Ma, G. Perry, X. Zhu, Mitochondria dysfunction in the pathogenesis of Alzheimer's disease: recent advances, Molecular Neurodegeneration 15(1) (2020) 30-51. https://doi.org/10.1186/s13024-020-00376-6.

[8] W.-X. Zong, J.D. Rabinowitz, E. White, Mitochondria and Cancer, Molecular Cell 61(5) (2016) 667-676. https://doi.org/10.1016/j.molcel.2016.02.011.

[9] A. Kannan, R.B. Wells, S. Sivakumar, S. Komatsu, K.P. Singh, B. Samten, J.V. Philley, E.R. Sauter, M. Ikebe, S. Idell, S. Gupta, S. Dasgupta, Mitochondrial Reprogramming Regulates Breast Cancer Progression, Clinical Cancer Research 22(13) (2016) 3348-3360. https://doi.org/10.1158/1078-0432.Ccr-15-2456.

[10] P.E. Porporato, N. Filigheddu, J.M.B.-S. Pedro, G. Kroemer, L. Galluzzi, Mitochondrial metabolism and cancer, Cell Research 28(3) (2018) 265-280. https://doi.org/10.1038/cr.2017.155.

[11] N.-E. Choi, J.-Y. Lee, E.-C. Park, J.-H. Lee, J. Lee, Recent Advances in Organelle-Targeted Fluorescent Probes, 26(1) (2021) 217-235. https://doi.org/10.3390/molecules26010217.

[12] S. Samanta, Y. He, A. Sharma, J. Kim, W. Pan, Z. Yang, J. Li, W. Yan, L. Liu, J. Qu, Fluorescent probes for nanoscopic imaging of mitochondria, Chem 5(7) (2019) 1697-1726. https://doi.org/doi.org/10.1016/j.chempr.2019.03.011.

[13] Q. Chen, H. Fang, X. Shao, Z. Tian, S. Geng, Y. Zhang, H. Fan, P. Xiang, J. Zhang, X. Tian, A dual-labeling probe to track functional mitochondria–lysosome interactions in live cells, Nature communications 11(1) (2020) 1-10. https://doi.org/10.1038/s41467-020-20067-6.

[14] Z. Xu, X. Huang, X. Han, D. Wu, B. Zhang, Y. Tan, M. Cao, S.H. Liu, J. Yin, J. Yoon, A visible and near-infrared,

dual-channel fluorescence-on probe for selectively tracking mitochondrial glutathione, Chem 4(7) (2018) 1609-1628. https://doi.org/10.1016/j.chempr.2018.04.003.
[15] J. Yin, M. Peng, W. Lin, Visualization of mitochondrial viscosity in inflammation, fatty liver, and cancer living mice by a robust fluorescent probe, Analytical chemistry 91(13) (2019) 8415-8421. https://doi.org/10.1021/acs.analchem.9b01293.
[16] J. Zhang, Q. Wang, Z. Guo, S. Zhang, C. Yan, H. Tian, W.H. Zhu, High-fidelity trapping of spatial–temporal mitochondria with rational design of aggregation-induced emission probes, Advanced Functional Materials 29(16) (2019) 1808153. https://doi.org/10.1002/adfm.201808153.
[17] R. Zhang, G. Niu, X. Li, L. Guo, H. Zhang, R. Yang, Y. Chen, X. Yu, B.Z. Tang, Reaction-free and MMP-independent fluorescent probes for long-term mitochondria visualization and tracking, Chemical science 10(7) (2019) 1994-2000. https://doi.org/10.1039/c8sc05119d.
[18] X. Zhang, Q. Sun, Z. Huang, L. Huang, Y. Xiao, Immobilizable fluorescent probes for monitoring the mitochondria microenvironment: a next step from the classic, Journal of Materials Chemistry B 7(17) (2019) 2749-2758. https://doi.org/10.1039/c9tb00043g.
[19] Z. Ye, L. Wei, X. Geng, X. Wang, Z. Li, L. Xiao, Mitochondrion-Specific Blinking Fluorescent Bioprobe for Nanoscopic Monitoring of Mitophagy, ACS Nano 13(10) (2019) 11593-11602. https://doi.org/10.1021/acsnano.9b05354.
[20] Y. Wang, X. Zhao, X. Gao, X. Nie, Y. Yang, X. Fan, Development of fluorescence imaging-based assay for screening cardioprotective compounds from medicinal plants, Analytica Chimica Acta 702(1) (2011) 87-94. https://doi.org/10.1016/j.aca.2011.06.020.
[21] H. Zhu, J. Fan, J. Du, X. Peng, Fluorescent Probes for Sensing and Imaging within Specific Cellular Organelles, Accounts of Chemical Research 49(10) (2016) 2115-2126. https://doi.org/10.1021/acs.accounts.6b00292.
[22] C. Zhou, W.-x. Zhao, F.-t. You, Z.-x. Geng, H.-s. Peng, Highly Stable and Luminescent Oxygen Nanosensor Based on Ruthenium-Containing Metallopolymer for Real-Time Imaging of Intracellular Oxygenation, ACS Sensors 4(4) (2019) 984-991. https://doi.org/10.1021/acssensors.9b00131.
[23] Y. Kurishita, T. Kohira, A. Ojida, I. Hamachi, Organelle-Localizable Fluorescent Chemosensors for Site-Specific Multicolor Imaging of Nucleoside Polyphosphate Dynamics in Living Cells, Journal of the American Chemical Society 134(45) (2012) 18779-18789. https://doi.org/10.1021/ja308754g.
[24] M.H. Lee, N. Park, C. Yi, J.H. Han, J.H. Hong, K.P. Kim, D.H. Kang, J.L. Sessler, C. Kang, J.S. Kim, Mitochondria-Immobilized pH-Sensitive Off–On Fluorescent Probe, Journal of the American Chemical Society 136(40) (2014) 14136-14142. https://doi.org/10.1021/ja506301n.
[25] S. Burge, G.N. Parkinson, P. Hazel, A.K. Todd, S. Neidle, Quadruplex DNA: sequence, topology and structure, Nucleic Acids Research 34(19) (2006) 5402–5415. https://doi.org/10.1093/nar/gkl655.
[26] E.Y.N. Lam, D. Beraldi, D. Tannahill, S. Balasubramanian, G-quadruplex structures are stable and detectable in human genomic DNA, Nature Communications 4 (2013) 1796-1803. https://doi.org/10.1038/ncomms2792.
[27] A. Henderson, Y. Wu, Y.C. Huang, E.A. Chavez, F.B.J. Jesse Platt, J. Robert M. Brosh, D. Sen, P.M. Lansdorp, Detection of G-quadruplex DNA in mammalian cells, Nucleic Acids Research 45(10) (2017) 6252-6252. https://doi.org/10.1093/nar/gkt957.
[28] Y. Cheng, Y. Zhang, Z. Gong, X. Zhang, Y. Li, X. Shi, Y. Pei, H. You, High Mechanical Stability and Slow Unfolding Rates Are Prevalent in Parallel-Stranded DNA G-Quadruplexes, Journal of Physical Chemistry Letters 11(19) (2020) 7966–7971. https://doi.org/10.1021/acs.jpclett.0c02229.
[29] W. Long, B.-X. Zheng, Y. Li, X.-H. Huang, D.-M. Lin, C.-C. Chen, J.-Q. Hou, T.-M. Ou, W.-L. Wong, K. Zhang, Y.-J. Lu, Rational design of small-molecules to recognize G-quadruplexes of c-MYC promoter and telomere and the evaluation of their in vivo antitumor activity against breast cancer, Nucleic Acids Research 50(4) (2022) 1829-1848. https://doi.org/10.1093/nar/gkac090.
[30] D. C.Wallace, Mitochondrial DNA Variation in Human Radiation and Disease, Cell 163(1) (2015) 33-38.

https://doi.org/10.1016/j.cell.2015.08.067.
[31] W.-C. Huang, T.-Y. Tseng, Y.-T. Chen, C.-C. Chang, Z.-F. Wang, C.-L. Wang, T.-N. Hsu, P.-T. Li, C.-T. Chen, J.-J. Lin, P.-J. Lou, T.-C. Chang, Direct evidence of mitochondrial G-quadruplex DNA by using fluorescent anti-cancer agents, Nucleic Acids Research 43(21) (2015) 10102-10113. https://doi.org/10.1093/nar/gkv1061.
[32] A. Bedrat, L. Lacroix, J.-L. Mergny, Re-evaluation of G-quadruplex propensity with G4Hunter, Nucleic Acids Research 44(4) (2016) 1746–1759. https://doi.org/10.1093/nar/gkw006.
[33] S.K. Bharti, J.A. Sommers, J. Zhou, D.L. Kaplan, J.N. Spelbrink, J.-L. Mergny, J. Robert M. Brosh, DNA Sequences Proximal to Human Mitochondrial DNA Deletion Breakpoints Prevalent in Human Disease Form G-quadruplexes, a Class of DNA Structures Inefficiently Unwound by the Mitochondrial Replicative Twinkle Helicase*, Journal of Biological Chemistry 289(43) (2014) 29975-29993. https://doi.org/10.1074/jbc.M114.567073.
[34] H. Yang, Y. Zhou, J. Liu, G-quadruplex DNA for construction of biosensors, TrAC Trends in Analytical Chemistry 132 (2020) 116060. https://doi.org/10.1016/j.trac.2020.116060.
[35] L.-L. Li, H.-R. Xu, K. Li, Q. Yang, S.-L. Pan, X.-Q. Yu, Mitochondrial G-quadruplex targeting probe with near-infrared fluorescence emission, Sensors and Actuators B: Chemical 286 (2019) 575 - 582. https://doi.org/10.1016/j.snb.2019.01.169.
[36] M.-H. Hu, Molecular engineering of a near-infrared fluorescent ligand for tracking mitochondrial DNA G-quadruplexes, Analytica Chimica Acta 1169 (2021) 338600. https://doi.org/10.1016/j.aca.2021.338600.
[37] X. Wang, L. Ge, Y. Yu, S. Dong, F. Li, Highly sensitive electrogenerated chemiluminescence biosensor based on hybridization chain reaction and amplification of gold nanoparticles for DNA detection, Sensors and Actuators B: Chemical 220 (2015) 942-948. https://doi.org/10.1016/j.snb.2015.06.032.
[38] Y. Zhao, C. Chang, P. Gai, L. Han, F. Li, B. Li, One-step synthesis of fluorescent organic nanoparticles: The application to label-free ratiometric fluorescent pH sensor, Sensors and Actuators B: Chemical 273 (2018) 1479-1486. https://doi.org/10.1016/j.snb.2018.07.047.
[39] M. Zuffo, A. Guédin, E.-D. Leriche, F. Doria, V. Pirota, V. Gabelica, J.-L. Mergny, M. Freccero, More is not always better: finding the right trade-off between affinity and selectivity of a G-quadruplex ligand, Nucleic Acids Research 46(19) (2018) 115-127. https://doi.org/10.1093/nar/gky607.
[40] X. Dan, M. Babbar, A. Moore, N. Wechter, J. Tian, J.G. Mohanty, D.L. Croteau, V.A. Bohr, DNA damage invokes mitophagy through a pathway involving Spata18, Nucleic Acids Research 48(12) (2020) 6611-6623. https://doi.org/10.1093/nar/gkaa393.
[41] J.-J. Cao, Y. Zheng, X.-W. Wu, C.-P. Tan, M.-H. Chen, N. Wu, L.-N. Ji, Z.-W. Mao, Anticancer Cyclometalated Iridium(III) Complexes with Planar Ligands: Mitochondrial DNA Damage and Metabolism Disturbance, Journal of Medicinal Chemistry 62(7) (2019) 3311-3322. https://doi.org/10.1021/acs.jmedchem.8b01704.
[42] H. Chen, H. Sun, S. Zhang, W. Yan, Q. Li, A. Guan, J. Xiang, M. Liu, Y. Tang, Monitoring autophagy in live cells with a fluorescent light-up probe for G-quadruplex structures, Chemical Communications 55(35) (2019) 5060-5063. https://doi.org/10.1039/C9CC01263J.
[43] D. Varshney, J. Spiegel, K. Zyner, D. Tannahill, S. Balasubramanian, The regulation and functions of DNA and RNA G-quadruplexes, Nature Reviews Molecular Cell Biology 21(8) (2020) 459-474. https://doi.org/10.1038/s41580-020-0236-x.
[44] X. Guo, D. Yang, R. Sun, Q. Li, H. Du, Y. Tang, H. Sun, A cyanine dye supramolecular FRET switch driven by G-quadruplex to monitor mitophagy, Dyes and Pigments 192 (2021) 109429-109434. https://doi.org/10.1016/j.dyepig.2021.109429.
[45] B.-X. Zheng, W. Long, Y.-H. Zhang, X.-H. Huang, C.-C. Chen, D.-X. Zhong, M.-T. She, Z.-X. Chen, D.-P. Cai, Y.-J. Lu, W.-L. Wong, Rational design of Red fluorescent and selective G-quadruplex DNA sensing probes: The study of interaction signaling and the molecular structural relationship achieving high specificity, Sensors and Actuators B: Chemical 314 (2020) 128075-128086. https://doi.org/10.1016/j.snb.2020.128075.

[46] W. Long, B.-X. Zheng, X.-H. Huang, M.-T. She, A.-L. Liu, K. Zhang, W.-L. Wong, Y.-J. Lu, Molecular Recognition and Imaging of Human Telomeric G-Quadruplex DNA in Live Cells: A Systematic Advancement of Thiazole Orange Scaffold To Enhance Binding Specificity and Inhibition of Gene Expression, Journal of Medicinal Chemistry 64(4) (2021) 2125-2138. https://doi.org/10.1021/acs.jmedchem.0c01656.
[47] B.-X. Zheng, M.-T. She, W. Long, Y.-Y. Xu, Y.-H. Zhang, X.-H. Huang, W. Liu, J.-Q. Hou, W.-L. Wong, Y.-J. Lu, A small-sized benzothiazole–indolium fluorescent probe: the study of interaction specificity targeting c-MYC promoter G-quadruplex structures and live cell imaging, Chemical Communications 56(95) (2020) 15016-15022. https://doi.org/10.1039/D0CC06525K.
[48] J. Kypr, I. Kejnovská, D. Renčiuk, M. Vorlíčková, Circular dichroism and conformational polymorphism of DNA, Nucleic Acids Research 37(6) (2009) 1713-1725. https://doi.org/10.1093/nar/gkp026.
[49] Y. Zhu, J. Hou, X.-H. Huang, D.-X. Zhong, W. Long, W. Liu, Y.-J. Lu, K. Zhang, W.-L. Wong, Structural modification of nonspecific thiazole orange for ligand-DNA interaction study: Understanding the ligand recognition selectivity towards G4-DNA over duplex-DNA, Journal of Luminescence 226 (2020) 117488-117496. https://doi.org/10.1016/j.jlumin.2020.117488.
[50] N. Sun, C. Wang, M.-H. Xu, Y.-J. Lu, Y.-Y. Zheng, Y. Yan, X.-L. Guo, J. Hou, K. Zhang, L.G. Luyt, W.-L. Wong, C.-F. Chow, The interaction of a structural flexible small molecule with nucleic acid structures: Investigation of the origin of fluorescence signal discrimination in sensing and the utilization in live cell imaging, Sensors and Actuators B: Chemical 250 (2017) 543-551. https://doi.org/10.1016/j.snb.2017.05.018.
[51] Z.Y. Yu, W.H. Luo, X.C. Chen, S.B. Chen, J.H. Tan, Efficient and rational development of a new fluorescent probe specific for RNA G-quadruplex imaging in cells, Sensors and Actuators B Chemical 324 (2020) 128770. https://doi.org/10.1016/j.snb.2020.128770.
[52] T. Shibata, Y. Nakayama, Y. Katahira, H. Tai, Y. Moritaka, Y. Nakano, Y. Yamamoto, Characterization of the interaction between heme and a parallel G-quadruplex DNA formed from d(TTGAGG), Biochimica et Biophysica Acta (BBA) - General Subjects 1861(5, Part B) (2017) 1264-1270. https://doi.org/10.1016/j.bbagen.2016.11.005.
[53] Y. Cao, P. Ding, L. Yang, W. Li, Y. Luo, J. Wang, R. Pei, Investigation and improvement of catalytic activity of G-quadruplex/hemin DNAzymes using designed terminal G-tetrads with deoxyadenosine caps, Chemical Science 11(26) (2020) 6896-6906. https://doi.org/10.1039/D0SC01905D.
[54] X.-Y. Zhuang, Y.-G. Yao, Mitochondrial dysfunction and nuclear-mitochondrial shuttling of TERT are involved in cell proliferation arrest induced by G-quadruplex ligands, FEBS Letters 587(11) (2013) 1656-1662. https://doi.org/10.1016/j.febslet.2013.04.010.
[55] O.L.S. Walker, H. Gurm, R. Sharma, N. Verma, L.L. May, S. Raha, Delta-9-tetrahydrocannabinol inhibits invasion of HTR8/SVneo human extravillous trophoblast cells and negatively impacts mitochondrial function, Scientific Reports 11 (2021) 4029-4043. https://doi.org/10.1038/s41598-021-83563-9.
[56] H. Gewirtz, Myocardial Imaging for Mitochondrial Membrane Potential, JACC: Cardiovascular Imaging 5(7) (2012) 758-760. https://doi.org/10.1016/j.jcmg.2012.04.004.
[57] W. Zhang, R.T.K. Kwok, Y. Chen, S. Chen, E. Zhao, C.Y.Y. Yu, J.W.Y. Lam, Q. Zheng, B.Z. Tang, Real-time monitoring of the mitophagy process by a photostable fluorescent mitochondrion-specific bioprobe with AIE characteristics, Chemical Communications 51(43) (2015) 9022-9025. https://doi.org/10.1039/C5CC02486B.